Supporting Information for:

Optical Actuation of Inorganic/Organic Interfaces: Comparing Peptide-Azobenzene Ligand Reconfiguration on Gold and Silver Nanoparticles

J. Pablo Palafox-Hernandez,[1,#] Chang-Keun Lim,[2,3,#] Zhenghua Tang,[4,5,#] Kurt L. M. Drew,[1] Zak E. Hughes,[1] Yue Li,[6] Mark T. Swihart,[3,6] Paras N. Prasad,[2,3,7,], Marc R. Knecht,[4,*] and Tiffany R. Walsh[1,*]*

[1]Institute for Frontier Materials, Deakin University, Geelong, Victoria 3216, Australia, [2] Department of Chemistry, [3]Institute for Laser Photonics and Biophotonics, University at Buffalo (SUNY), Buffalo, New York 14260, United States, [4]Department of Chemistry, University of Miami, 1301 Memorial Drive, Coral Gables, Florida 33146, United States, [5] New Energy Research Institute, School of Environment and Energy, South China University of Technology, Guangzhou Higher Education Mega Centre, Guangzhou, China, 510006, [6]Department of Chemical and Biological Engineering, University at Buffalo (SUNY), Buffalo, New York 14260, United States and [7]Department of Chemistry, Korea University, Seoul 151-747, Korea.

(#: These authors contributed equally)

*To whom correspondence should be addressed:

PNP: pnprasad@buffalo.edu; MRK: knecht@miami.edu; TRW: tiffany.walsh@deakin.edu.au

Experimental Details:

Synthesis of (E)-4,4'-(diazene-1,2-diyl)bis(*N*-(2-(2,5-dioxo-2,5-dihydro-1H-pyrrol-1-yl)ethyl) benzamide) (MAM). Azobenzene-4,4'-dicarboxylic acid (**1**) (2.67 g, 9.9 mmol) and thionyl chloride (60 mL) were refluxed overnight at 85 ºC. The solution was evaporated three times from toluene and the solid azobenzene-4,4'-dicarboxylic acid chloride (**2**) was obtained (Yield: 98%). **2** (307 mg, 1 mmol) was dissolved in methylene chloride (10 mL) and mixed with a solution of *N*-(2-aminoethyl)maleimide hydrochloride (620 mg, 3.5 mmol) and TEA (0.7 mL) in methylene chloride (10 mL). The mixture was stirred overnight at room temperature and evaporated. The product was recrystallized from ethanol to give MAM as an orange powder (Yield: 45%). ^{1}H NMR (DMSO-d_6, 500 MHz, ppm): δ 8.76 (t, J = 6 Hz, 2H), 7.95 (s, J = 8H), 7.02 (s, 4H), 3.60 (t, J =5.5 Hz, 4H), 3.43(q, J = 5.5 Hz, 4H). ^{13}C NMR (DMSO-d_6, 75 MHz, ppm): δ 171.11, 165.72, 153.21, 136.98, 134.55, 128.43, 122.51, 37.73, 37.10. HR-MS (ESI$^+$): Calculated for $C_{26}H_{22}N_6O_6$: 514.50; Found: 514.16.

Peptide synthesis and MAM coupling. The AuBP1C and CAuBP1 peptides were synthesized using standard FMOC protocols on a TETRAS solid phase peptide synthesizer (CreoSalus). The peptide was cleaved from the resin, purified by reverse phase HPLC, and confirmed via MALDI-TOF mass spectrometry. Once the peptide was confirmed, coupling of the MAM at the incorporated cysteine residue proceeded. In a typical reaction, 27.0 mg of the peptide (either AuBP1C or CAuBP1) was dissolved in 4 mL of DMF, which was then added to a MAM solution in DMF (13.5 mg dissolved in 2 mL DMF). In this reaction, the molar ratio of MAM:peptide is 1:4, which promotes coupling of only one peptide per MAM. Once initiated, the reaction was stirred for 3 days, after which 150 mL of ethyl ether was added, resulting in precipitation of a yellow solid.

Due to differential solubilities, ether precipitation resulted in sample purification from unreacted MAM. The sample was centrifuged to form a pellet, the supernatant was removed, and more ethyl ether was added. This process was repeated two more times to increase peptide final purity. After centrifuge purification, the sample was purified using reverse phase HPLC and confirmed with MALDI-TOF mass spectrometry.

Nanoparticle synthesis and characterization. In a typical synthesis, 10 μL of a 0.1 M aqueous solution of $HAuCl_4$ or $AgNP_3$ was diluted in 2.96 mL of water and then mixed with 2 mL of a 0.25 mM aqueous solution of AuBP1C-MAM or MAM-CAuBP1 in a vial, resulting in a Au:MAM-peptide ratio of 2. The solution was thoroughly mixed for at least 15 min, followed by injection of 30 μL of an ice cold, freshly prepared, 0.1 mM NaBH4 aqueous solution. Upon the addition of reducing agent, the color of the Au solution immediately changed from pale yellow to wine red, while the color of the Ag solution changed from light yellow to bright yellow. The reaction was allowed to continue undisturbed for 1 h at room temperature to ensure complete reduction. To prepare the materials using the MAM-peptides in the trans form, the process was carried out on the benchtop under ambient illumination; however, to generate structures in the presence of the cis MAM-peptide, the hybrids solutions were illuminated with a 365 nm UV-lamp for 1h before mixing with the metal ion solutions, and then the reaction was carried out under UV illumination. In this case, photoisomerization of the azobenzene unit to the cis configuration was confirmed using UV-vis absorbance prior to NP fabrication to ensure the appropriate molecular configuration (see Figure S1). The size and shape of the Au nanoparticles were characterized using a JEOL JEM-2010 TEM operating at a working voltage of 200 kV. The specimen was prepared by drop-casting 15 μL of the Au solution onto a carbon-coated Cu TEM

grid. The optical absorbance spectra of Au nanoparticles were measured using a Shimadzu UV-3101PC spectrometer employing a 1 cm quartz cuvette.

Computational Details:

Metadynamics Simulations:

We performed four well-tempered metadynamics[1] simulations describing the adsorption of either the *cis* or the *trans* conformations of the MAM unit alone (*i.e.* without the peptide) at the aqueous Au(111) and Ag(111) interfaces. The PLUMED plugin[2] was used to apply the metadynamics approach in these simulations. All of these simulations were carried out in the Canonical (NVT) ensemble at a temperature of 300 K with the Nosé-Hoover thermostat,[3-4] using GROMACS version 4.6.1.[5] The polarizable GolP-CHARMM[6-7] or AgP-CHARMM[8] force-fields were used in partnership with the CHARMM22*[9-10] and the modified TIP3P[11-12] force-fields. Details of the force-field modifications required to model the maleimide-azobenzene-maleimide (MAM) moiety were provided in a previous study.[13] The metal atoms in the slab (five atomic layers thick) were held fixed in position throughout the simulations, with lateral slab dimensions of 58.6×60.9 Å and 58.9×61.2 Å for Au and Ag respectively, and an inter-slab spacing of over 50 Å in each case. The dimension of the cell perpendicular to the slab was adjusted such that the density of liquid water in the central region between the slabs was consistent with the liquid water density at room temperature and ambient pressure. Each metadynamics simulation used a time step of 1 fs, with the Lennard-Jones nonbonded interactions switched off between 9.0 and 10.0 Å, and a cutoff of 11.0 Å used for the particle mesh Ewald (PME)[14] summation. The potential bias was applied to the position of the center of mass of the central N—N bond of the azobenzene substituent of the MAM, along the direction perpendicular to the metal surface. Gaussians of 0.5 Å width were deposited every 1 ps for 300 ns, and the initial Gaussian height was set to 0.240 kJ mol^{-1}. A well-tempered metadynamics bias factor of 50 was used. Each system consisted of the MAM molecule (in either the *cis* or *trans* state), the Au(111) or Ag(111) slab and 6093 TIPS3P waters.

Extraction of Adsorption Free Energies:

In the limit of an infinite metadynamics simulation ($t \rightarrow \infty$), the bias added during a metadynamics simulation approaches the negative of the free energy of the system, $V(X, t) \rightarrow -$

$G(X, t)$, where V, G and X are the metadynamics bias added, the free energy of the system and its co-ordinates, respectively. The symmetrical nature of our simulation set-up means that two estimates of the binding affinity of the MAM unit for the metallic surface could be generated per run; adsorption to the top face of the metal slab ($\Delta G_{ads,t}$) and adsorption to the underside of the periodic neighboring slab ($\Delta G_{ads,b}$) respectively (referred to herein as the bottom face). $\Delta G_{ads,t}$ and $\Delta G_{ads,b}$ were estimated using:

$$\Delta G = -k_B T ln\left(\frac{c_{ads,t}}{c_{bulk}}\right) \qquad (1)$$

$$\Delta G = -k_B T ln\left(\frac{c_{ads,b}}{c_{bulk}}\right) \qquad (2)$$

where $c_{ads,t}$ is the concentration of adsorbed peptide at the top face, $c_{ads,b}$ is the concentration of the adsorbed peptide at the bottom face, and c_{bulk} is the peptide concentration in the bulk. These concentrations are given by:

$$c_{ads,t} = \frac{1}{z_0 - z_{min}} \int_{z_{min}}^{z_0} exp\left[-G(X, t_f)\Big/ k_B T\right] dX \qquad (3)$$

$$c_{ads,b} = \frac{1}{z_{max} - z_1} \int_{z_1}^{z_{max}} exp\left[-G(X, t_f)\Big/ k_B T\right] dX \qquad (4)$$

$$c_{bulk} = \frac{1}{z_1 - z_0} \int_{z_0}^{z_1} exp\left[-G(X, t_f)\Big/ k_B T\right] dX \qquad (5)$$

where z_0 and z_1 indicate the values of the CV for which the MAM is considered to be in the 'bulk' solution (*i.e.* the MAM was defined as not adsorbed for $z_0 < z < z_1$, and was defined as adsorbed for all other values of z). z_{min} is the z coordinate of the top (upper side) of the metal slab, and correspondingly z_{max} is the z coordinate bottom surface of the underside of slab as its periodic image. T is the temperature and t_f = 300 ns, the duration of the metadynamics simulations performed in this work. Specifically, z_0 was defined using the final symmetrized free energy profiles of each system to be the minimum value of the CV for which $G(X, t_f) > -4$ kJ mol^{-1}; z_1 was then assigned the same distance from the bottom surface of the periodic image of the slab. Herein, we quote our calculated binding free energies as ΔG_{ads}, the mean of $\Delta G_{ads,t}$ and $\Delta G_{ads,b}$. The associated error was defined as half the difference between $\Delta G_{ads,t}$ and $\Delta G_{ads,b}$.

Replica Exchange with Solute Tempering Molecular Dynamics Simulations:

System Setup: Each system (8 systems in total) comprised one 5-layer Ag or Au slab presenting the (111) surface on both sides of the slab, one peptide chain, ~6600 water molecules, and, as required, counter-ions (in the form of Na^+ and Cl^- ions) to ensure overall charge neutrality of the simulation cell. Each peptide was modelled with the zwitterionic form of the N- and C-termini (*i.e*. no capping groups), consistent with the experimentally synthesized peptides. Each residue in each hybrid molecule was assigned a protonation state consistent with a solution pH of ~7. We used an orthorhombic periodic cell; the gold slab had lateral dimensions 58.6 Å x 60.9 Å, with an inter-slab spacing perpe32ndicular to the slab surface in excess of 55 Å (such that the perpendicular dimension of the cell was 67.6 Å). The height of the cell was adjusted such that the density of liquid water in the central region between the slabs was consistent with the liquid water density at room temperature and ambient pressure. Periodic boundary conditions were applied in all three dimensions. All simulations were performed in the Canonical (*NVT*) ensemble, at a temperature of 300K, maintained using the Nosé-Hoover thermostat,[3-4] with a coupling constant of τ = 0.4 ps. Newton's equations of motion were solved using the leapfrog algorithm with an integration time-step of 1fs. Coordinates and velocities were saved every 1000 steps (1ps). Long-ranged electrostatic interactions were treated using Particle-mesh Ewald (PME),[14] with a cut-off at 11 Å, whereas a force-switched cut-off, starting at 9 Å and ending at 10 Å was used for Lennard-Jones non-bonded interactions.

The GolP-CHARMM[6-7] and AgP-CHARMM[8] force-fields were used to model the Au and Ag slabs respectively. The peptide was described using the CHARMM22*[9-10] force-field, and water was described using TIPS3P.[11-12] All metal atoms in the slab were held fixed in space during these simulations, with only the metal atom dipoles able to freely rotate. Random initial dipole positions were used throughout. Our recent tests indicate that there is very little difference between binding free energies obtained using a rigid substrate, *vs*. using a slab where all atoms can move.[15] Details of the force-field modifications required to model the maleimide-azobenzene-maleimide (MAM) moiety were provided in a previous study.[13]

REST Details: Our implementation of REST exploits the replica exchange and free energy perturbation theory functionalities within Gromacs 4.5.5.[5] Details of the Terakawa implementation[16] of REST have been given by us previously.[17] In our REST simulations, we

spanned an 'effective temperature' window of 300-430K with 16 replicas. The initial configurations for each replica cover a range of secondary structures, including α-helix, β-turn, polyproline II and random coil conformations for the peptide component of the molecule, and either the *trans* or the *cis* conformation for the MAM component of the molecule. The adsorbate structure for each replica was initially placed so that at least one peptide atom was within ~3Å distance from the top surface of either the Au slab or the Ag slab. The 16 values of lambda used to scale our force-field were:

λ_j = 0.0000, 0.057, 0.114, 0.177, 0.240, 0.310, 0.382, 0.458, 0.528, 0.597, 0.692, 0.750, 0.803, 0.855, 0.930, 1.0000.

Prior to each REST simulation, initial configurations were equilibrated at their target potential for 0.5 ns, with no exchange moves attempted during this time. The interval between exchange attempts set to 1000 MD steps (every 1 ps). All production REST simulations were run for a total of 25 $\times 10^6$ MD steps (25 ns).

Evidence of the sampling efficacy of the REST approach is given in Figure S4, where our example shows the typical high degree of mobility of the replicas through lambda space.

In Figure S5, we show an example of evidence used to determine sample equilibration, namely the number of clusters *vs.* REST MD steps for the unscaled, reference replica (λ = 0.000).

REST MD clustering analysis: Detailed analysis was carried out on the constant-ensemble run at an effective temperature of 300K (herein referred to as the reference trajectory). We classified the Boltzmann-weighted ensemble from our reference trajectories into groups of like structures, on the basis of similarity of their backbone structures, *via* the Daura clustering algorithm[18] with a root mean-squared deviation (RMSD) cutoff between the positions all peptide backbone atoms. We used two definitions of the backbone; in the first, the backbone was denoted by the peptide backbone atoms plus the atoms along the mid-line of the MAM unit (we denote this as clustering over the entire molecule); in the second, we considered only the backbone of the AuBP1 sequence within the hybrid molecule, to enable direct comparison with our previously published data on the parent peptide. In the former case, the RMSD cutoff was 3 Å, in the latter we used a cutoff of 2 Å. In general, RMSD cutoffs used in clustering analyses are size-extensive, such that the cutoff should be adjusted to be commensurate with the size of the molecule. The cutoff of 2

Å was identified via extensive testing conducted on dodecapeptides[17] from which we found a cutoff of 2 Å to yield an appropriately sensible balance between resolution and meaningful structural similarity. The MAM-peptide hybrid is a larger molecule and therefore it is appropriate to use a larger cutoff in this case. Again, our extensive testing identified a cutoff of 3Å to be reasonable in this instance. We emphasize here that it is not appropriate to directly compare clustering data obtained with different cutoffs. We performed our clustering analysis over the entire 25 ns trajectory in each case. The population of a given cluster was calculated as the percentage fraction of the number of frames that were assigned membership of that cluster, divided by the total number of frames in the trajectory.

REST MD Contact Residue analysis:

We define a contact residue as a residue that maintains persistent contact with the surface. To quantify persistent contact, first, for each reference trajectory, we calculated the distance between the topmost layer of the gold surface and each residue in the sequence. On the basis of these data, distance cut-offs were established to identify a range of separations where each particular residue, including the MAM unit, was in immediate contact with the gold surface. We then calculated the fraction of frames in the reference trajectory for which each residue was found within the contact range of surface-residue separation. We then defined a residue to be a contact residue if that residue was found to bind persistently to the surface. Our definition of persistent contact was satisfied if the given residue was found within contact range for 60% of more of the last 5 ns of the reference trajectory. Further details including the data used to establish the cutoffs, and further analysis based on variation of both the contact cutoff distance and the percentage of frames required to satisfy our definition of a contact residue can be found in our previous work[13, 19].

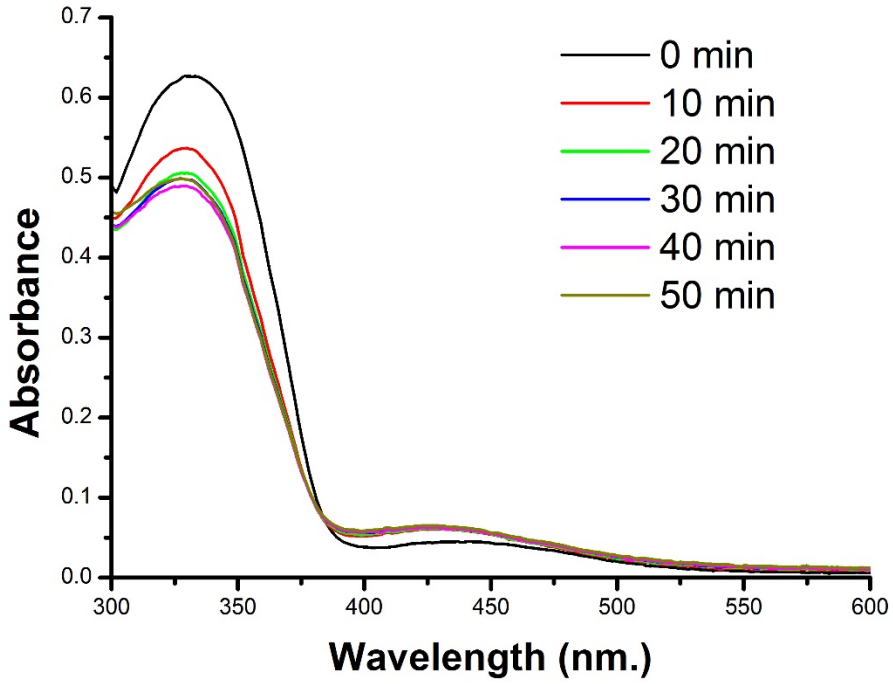

Figure S1: Time-dependent *trans* to *cis* isomerization of 0.1 mM AuBP1C-MAM upon 365nm UV-lamp illumination.

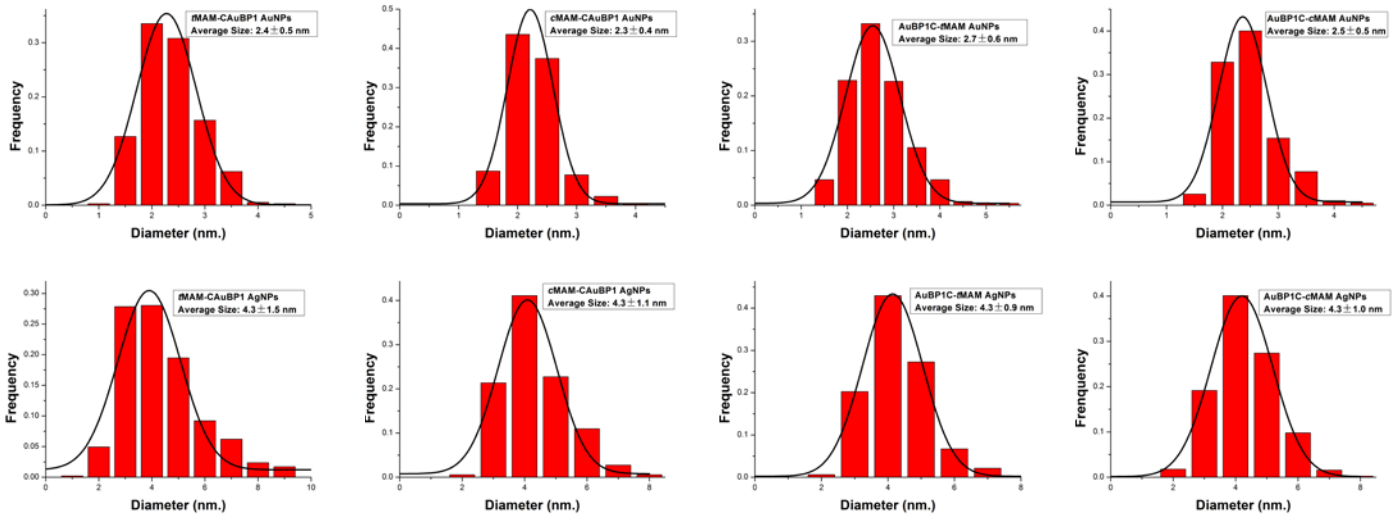

Figure S2: Size distribution obtained from TEM analysis of the Au and Ag nanoparticles prepared using the indicated peptides.

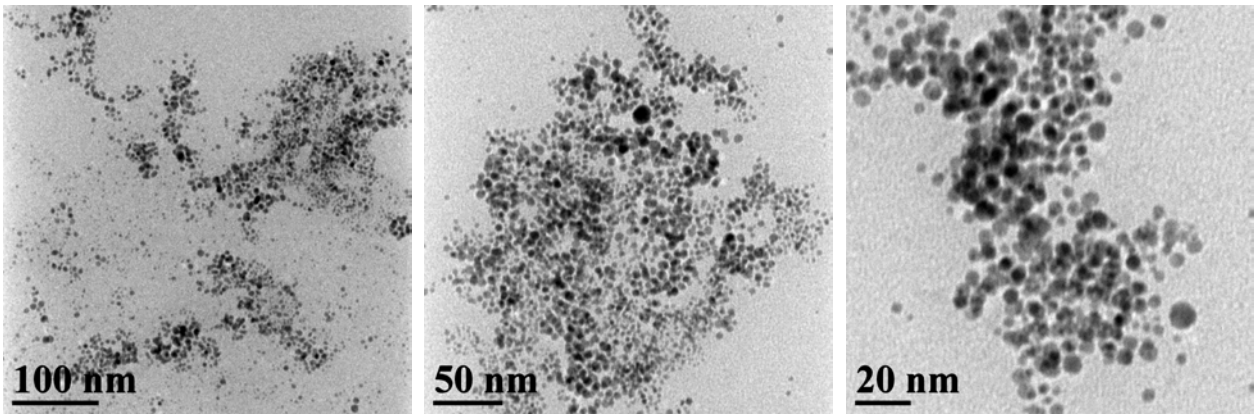

Figure S3: Larger nanoparticle aggregates synthesized with AuBP1C-MAM using a combination of $NaBH_4$ and ascorbic acid as reducing agents.

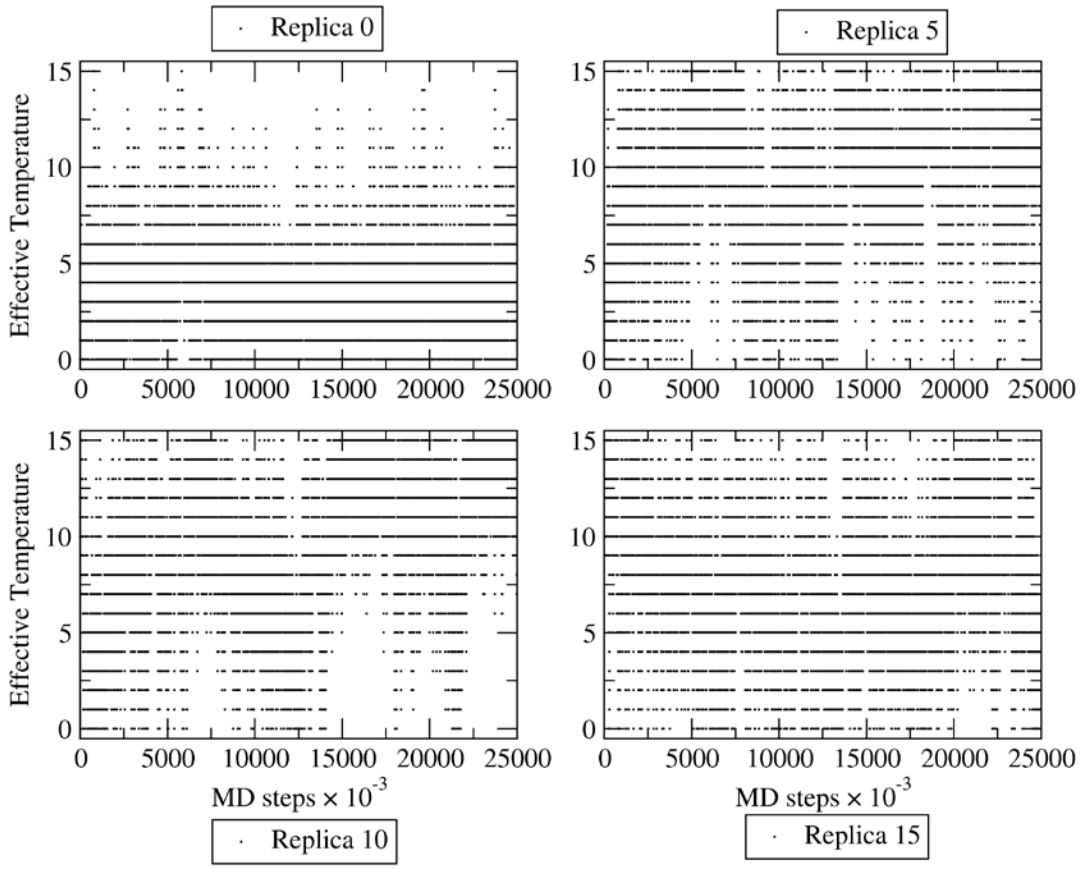

Figure S4: Exemplar REST simulation effective temperature mobilities for four out of the sixteen replicas, for the *t*MAM-CAuBP1 hybrid adsorbed at the aqueous Au(111) interface.

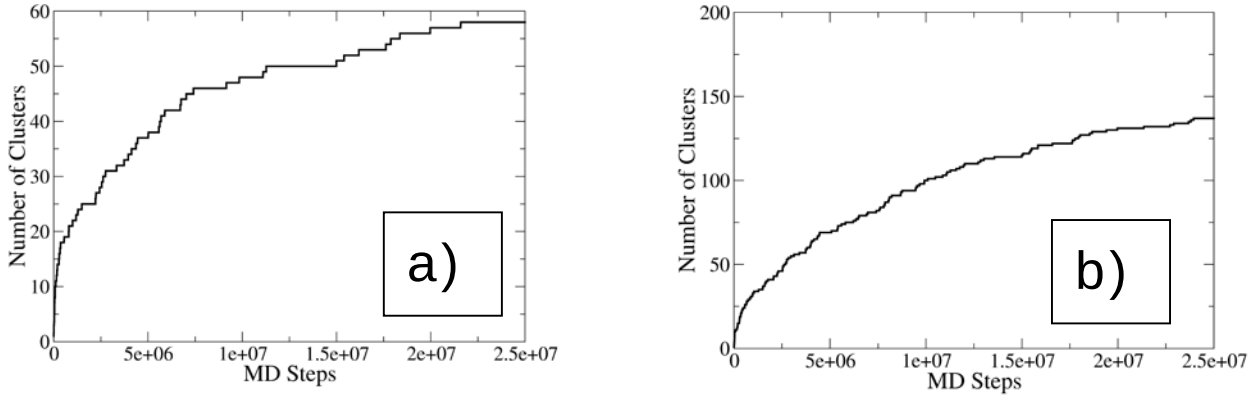

Figure S5: Number of clusters as a function of REST MD steps, shown for the *t*MAM-CAuBP1 hybrid molecule adsorbed at the aqueous Au(111) interface; **a)** clustered over the entire hybrid molecule, **b)** clustered over the AuBP1 backbone only.

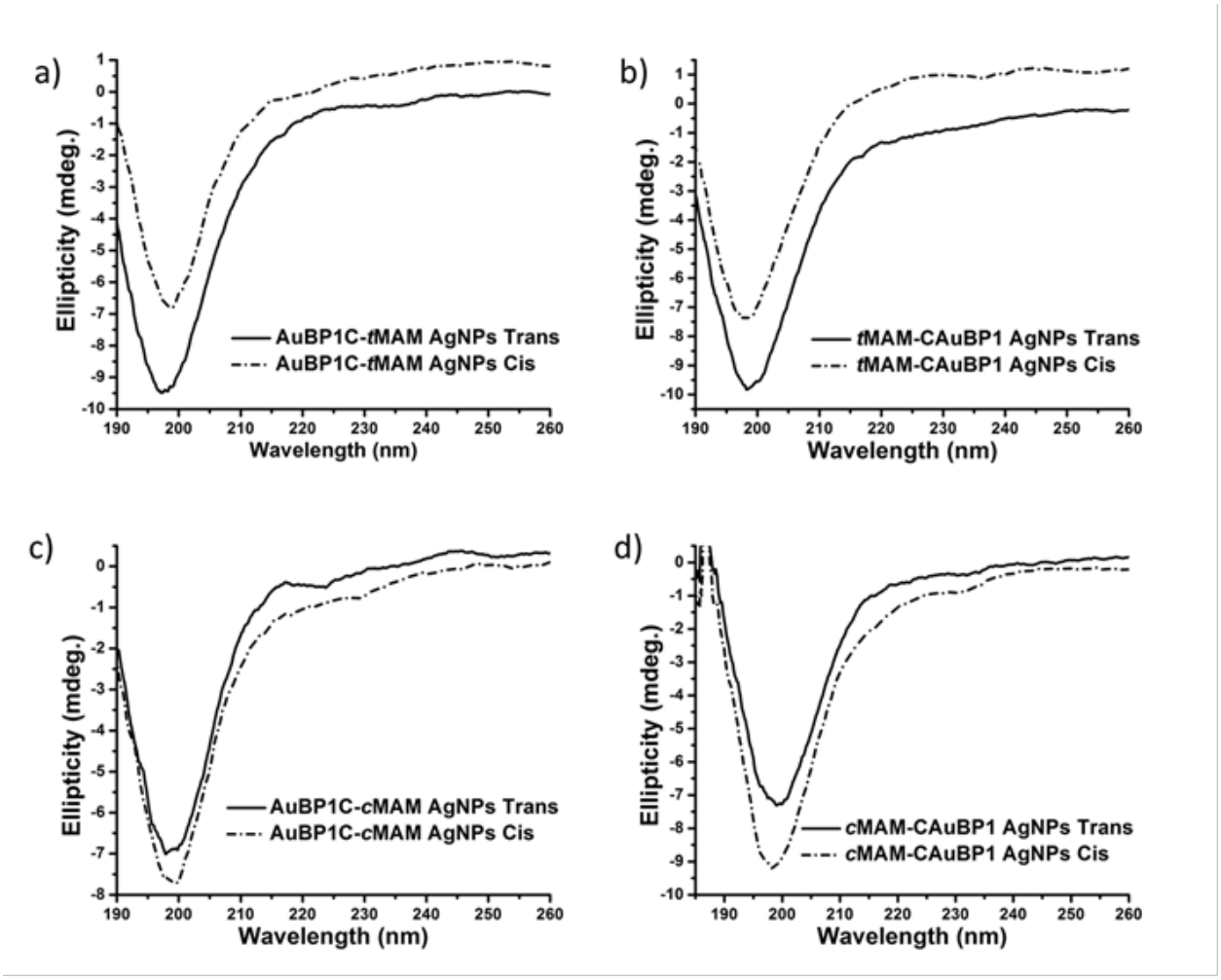

Figure S6: CD spectra of peptides in *trans* (solid curves) and *cis* (dashed curves) conformations bound on Ag nanoparticles synthesized with (a) AuBP1C-MAM in *trans* form, (b) MAM-CAuBP1 in *trans* form, (c) AuBP1C-MAM in *cis* form, and (d) MAM-CAuBP1 in *cis* form, respectively.

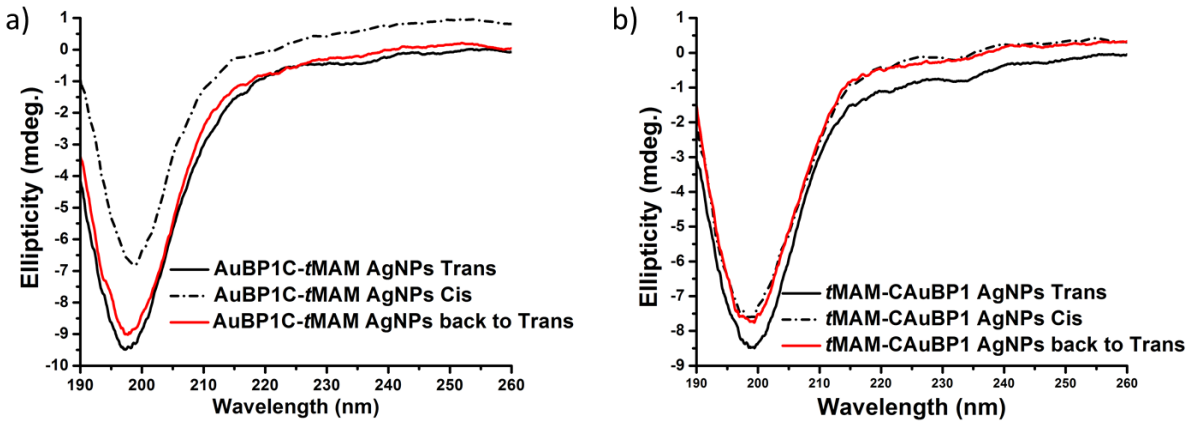

Figure S7: Reversibility of secondary structure changes of Ag nanoparticle-bound peptides in the case of (a) AuBP1C-MAM and (b) MAM-CAuBP1. The peptides were initially switched from *trans* (black solid curves) to *cis* form (black dashed curves), and then switched back to *trans* form (red solid curves).

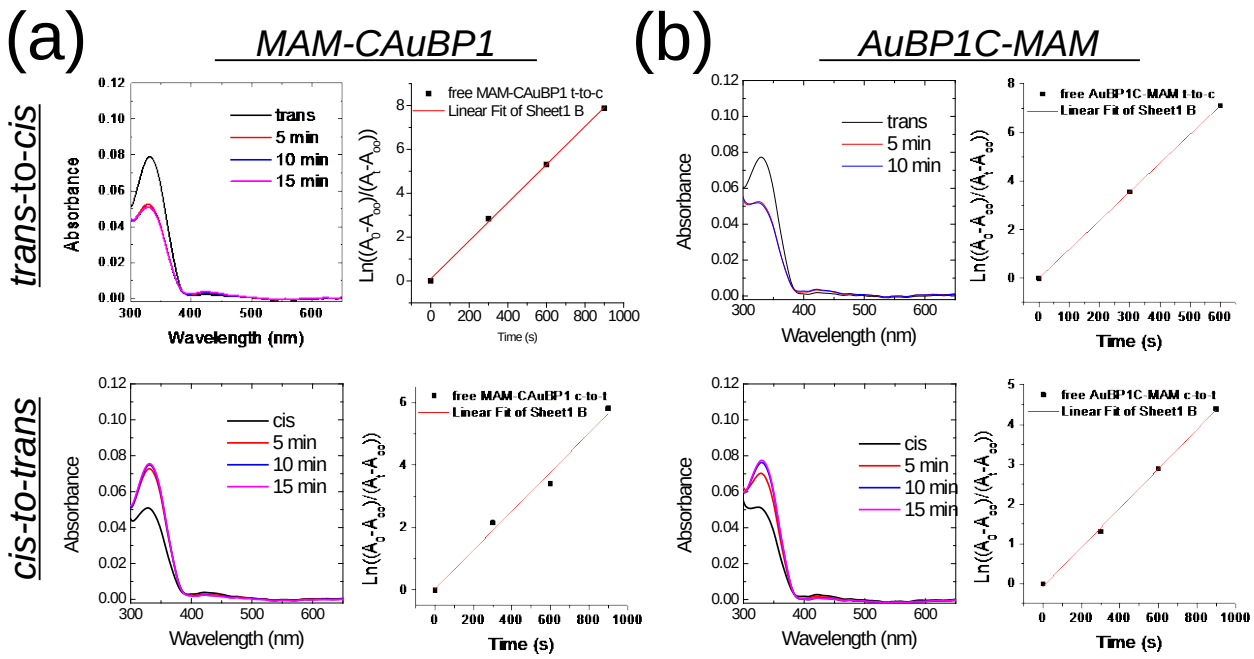

Figure S8: Time-dependent photoswitching analysis of the free (a) MAM-CAuBP1 and (b) AuBP1C-MAM in water. Left graphs show time-dependent absorption spectra upon 340 nm (*trans* to *cis*) and 440 nm (*cis* to *trans*) illumination. Right graphs show plots of first-order rate law.

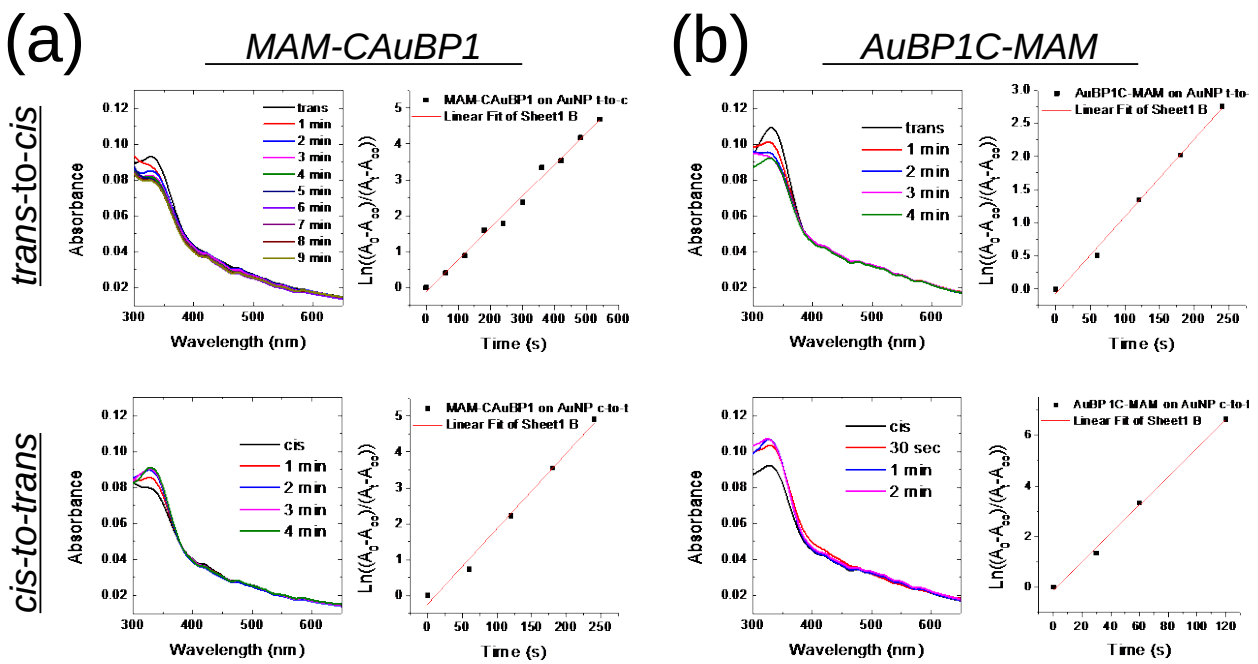

Figure S9: Time-dependent photoswitching analysis of the (a) MAM-CAuBP1 and (b) AuBP1C-MAM on Au NP. Left graphs show time-dependent absorption spectra upon 340 nm (*trans* to *cis*) and 440 nm (*cis* to *trans*) illumination. Right graphs show plots of first-order rate law.

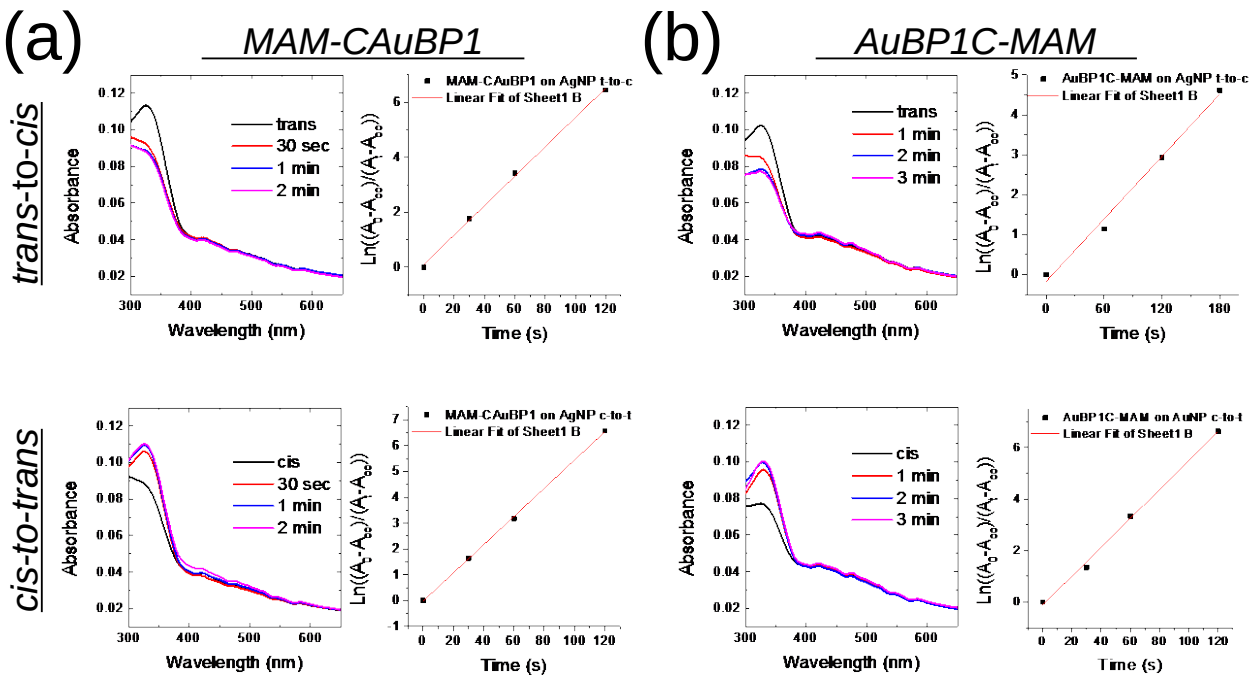

Figure S10: Time-dependent photoswitching analysis of the (a) MAM-CAuBP1 and (b) AuBP1C-MAM on Ag NP. Left graphs show time-dependent absorption spectra upon 340 nm (*trans* to *cis*) and 440 nm (*cis* to *trans*) illumination. Right graphs show plots of first-order rate law.

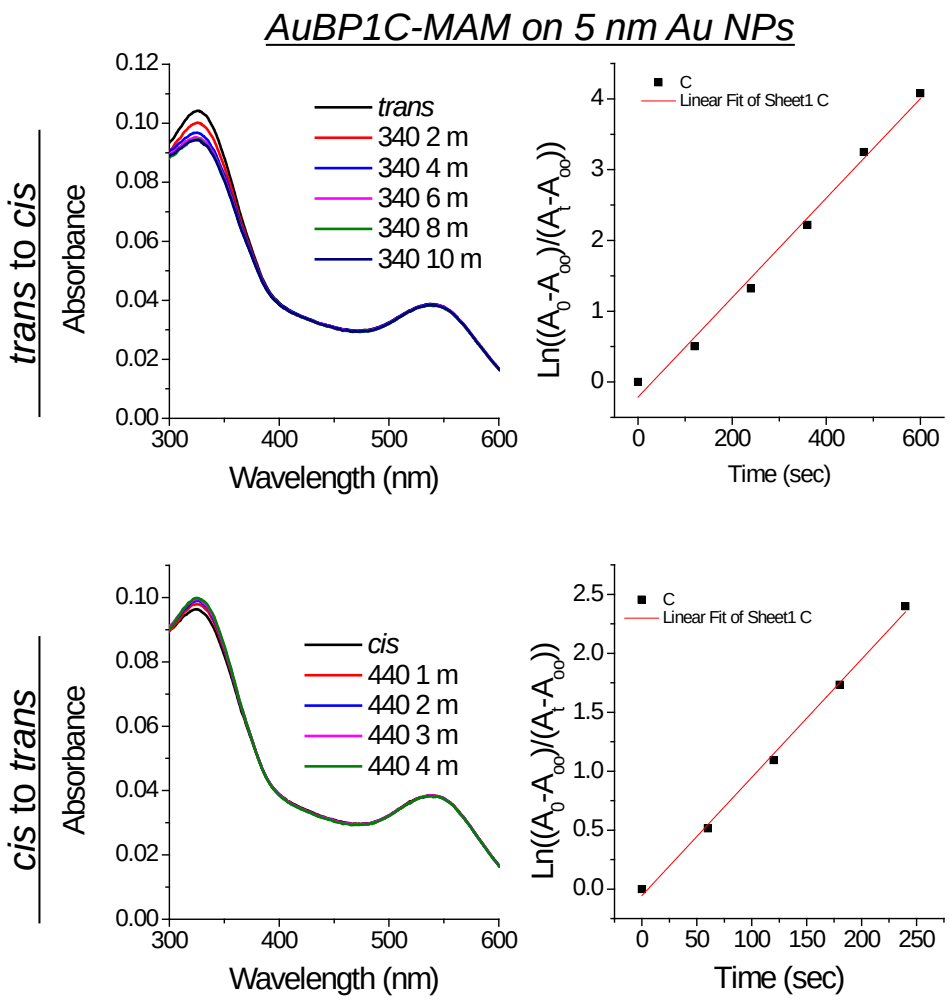

Figure S11: Time-dependent photoswitching analysis of 5 nm AuBP1C-MAM capped Au NP. Left graphs show time-dependent absorption spectra upon 340 nm (*trans* to *cis*) and 440 nm (*cis* to *trans*) illumination. Right graphs show plots of first-order rate law.

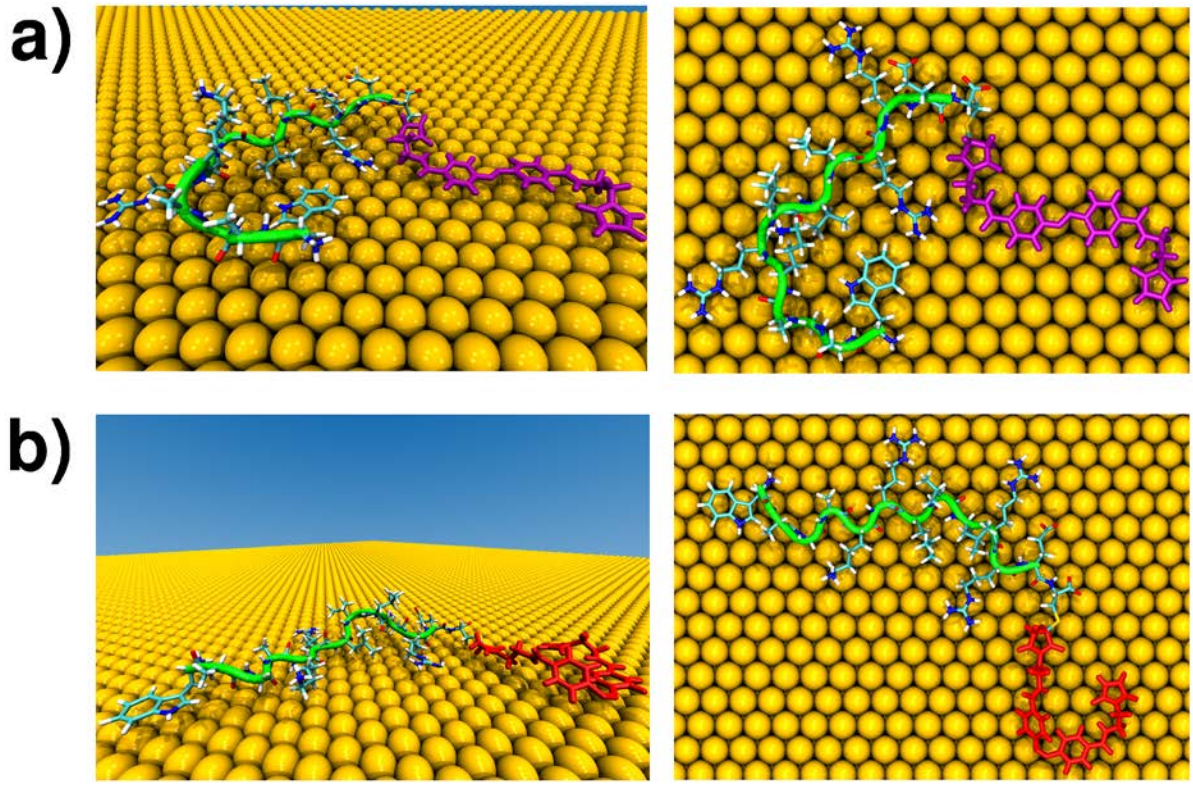

Figure S12: Structures corresponding with the most populated cluster (see Methods) for the AuBP1C-MAM hybrid biomolecule adsorbed at the aqueous Au(111) interface predicted from REST MD simulations. The *trans* and *cis* forms of the MAM unit are shown in purple and red respectively. Water molecules are not shown for clarity.

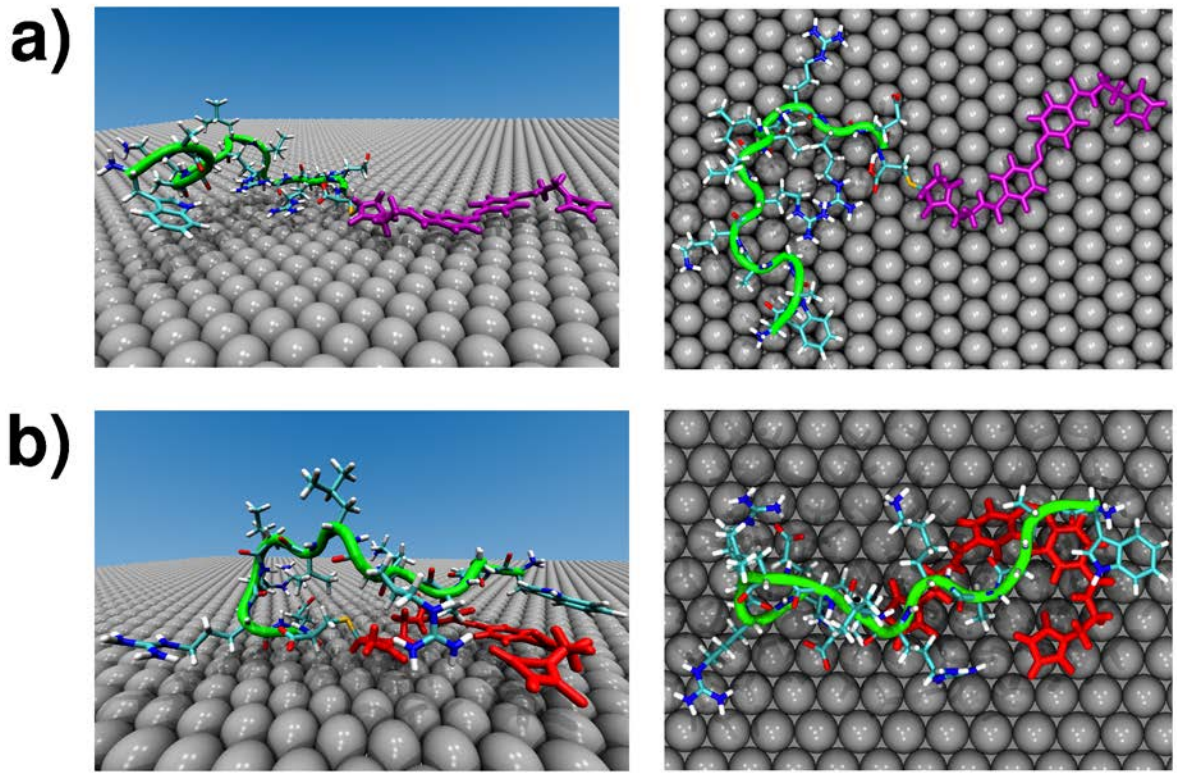

Figure S13: Structures corresponding with the most populated cluster (see Methods) for the AuBP1C-MAM hybrid biomolecule adsorbed at the aqueous Ag(111) interface predicted from REST MD simulations. The *trans* and *cis* forms of the MAM unit are shown in purple and red respectively. Water molecules are not shown for clarity.

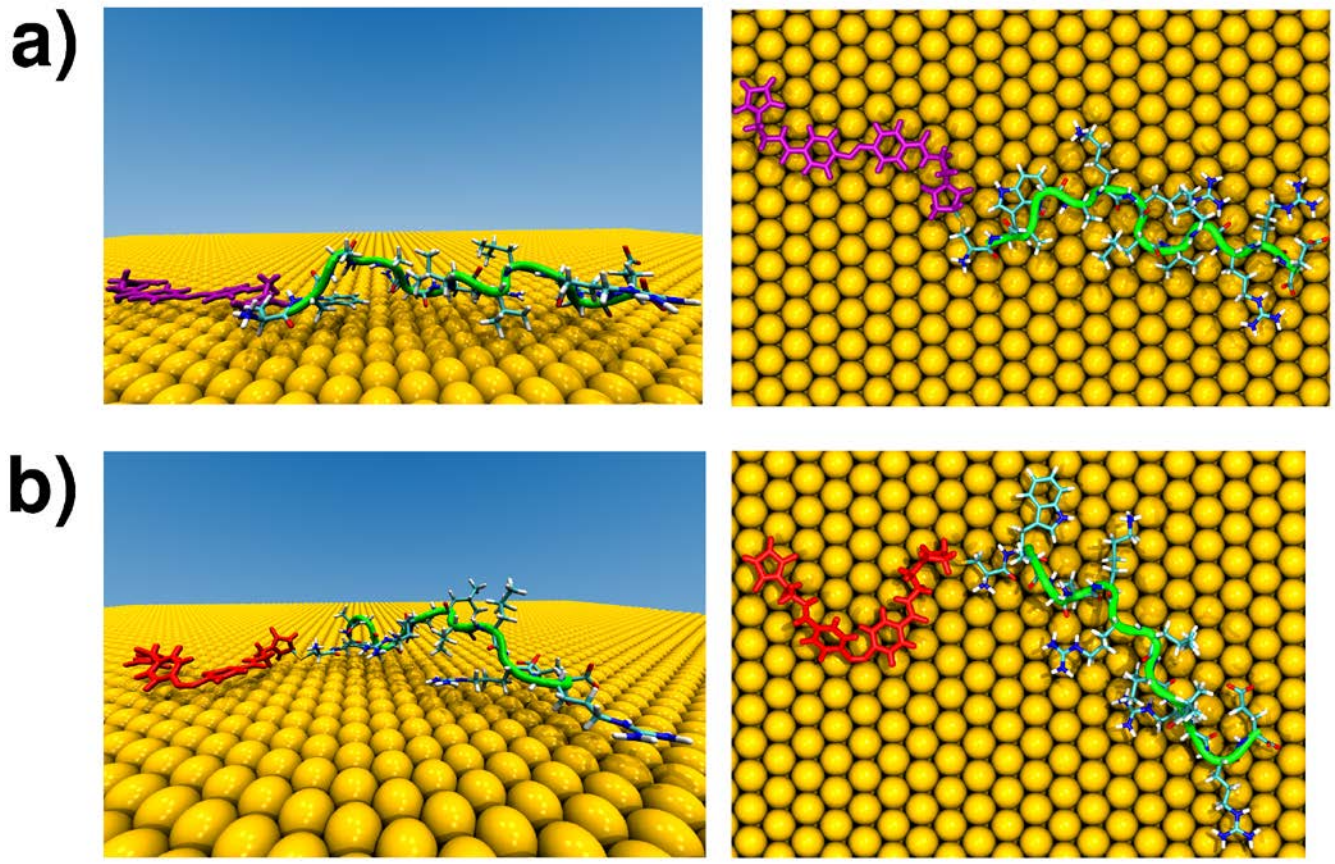

Figure S14: Structures corresponding with the most populated cluster (see Methods) for the MAM-CAuBP1 hybrid biomolecule adsorbed at the aqueous Au(111) interface predicted from REST MD simulations. The *trans* and *cis* forms of the MAM unit are shown in purple and red respectively. Water molecules are not shown for clarity.

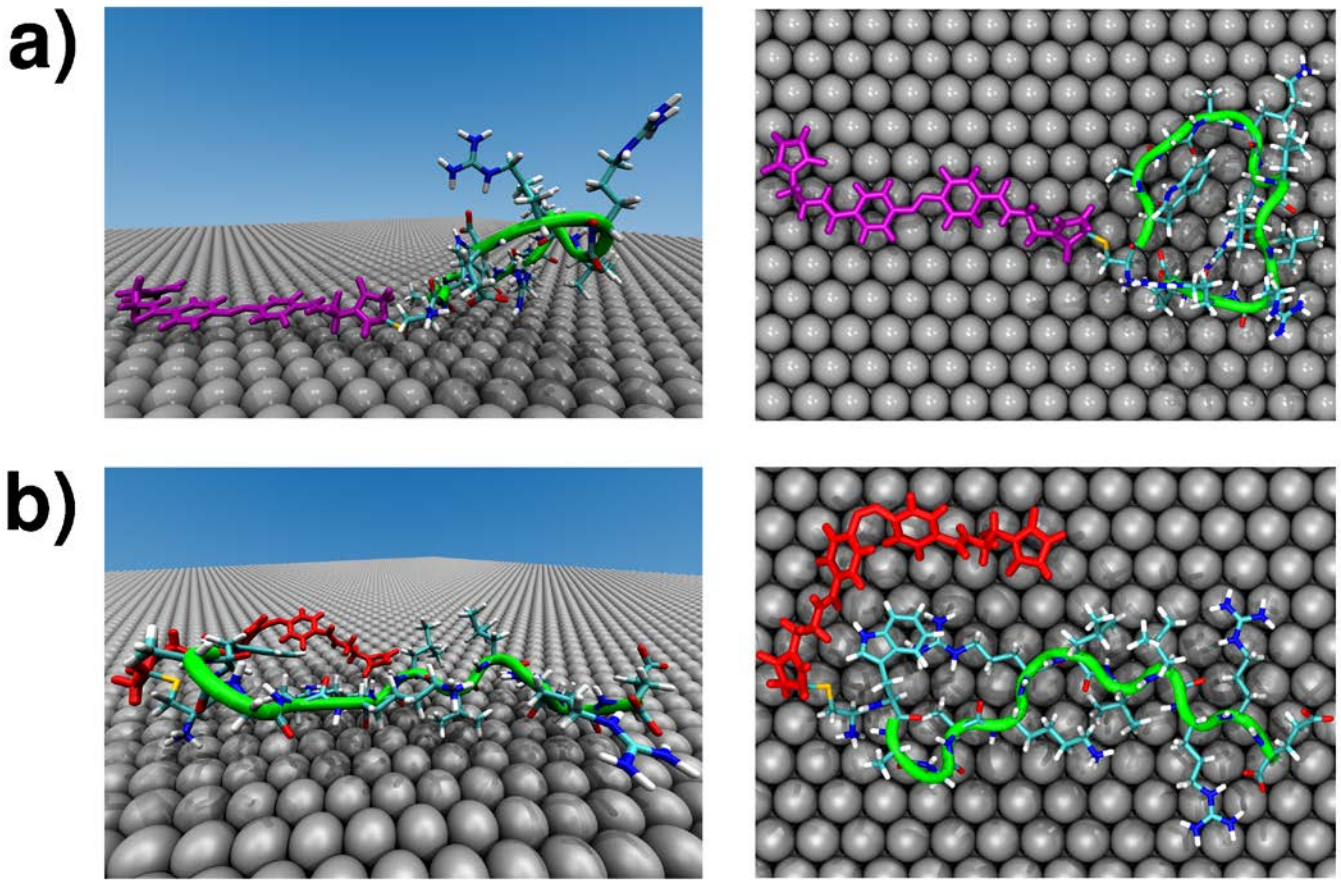

Figure S15: Structures corresponding with the most populated cluster (see Methods) for the MAM-CAuBP1 hybrid biomolecule adsorbed at the aqueous Ag(111) interface predicted from REST MD simulations. The *trans* and *cis* forms of the MAM unit are shown in purple and red respectively. Water molecules are not shown for clarity.

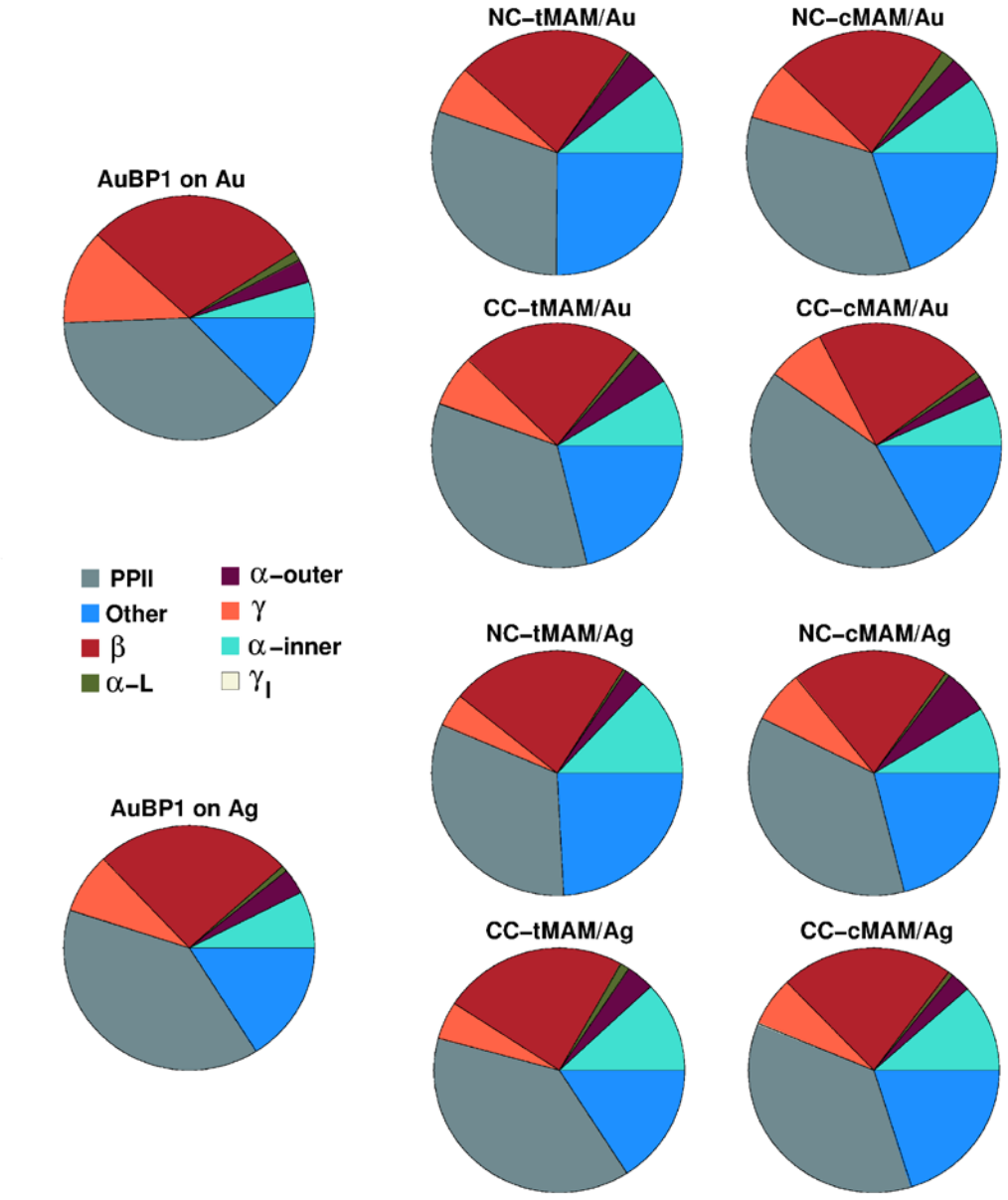

Figure S16: Population of secondary structure motifs taken from Ramachandran analysis of the reference replica REST trajectories for each case.

Table S1: First-order kinetic constant (k_{iso}) of the isomerization.

Molecule	Nanoparticles	Isomerization	k_{iso} /s^{-1}
MAM-CAuBP1		t-to-c	0.036 ± 0.006
MAM-CAuBP1		c-to-t	0.019 ± 0.0073
MAM-CAuBP1	Au NP	t-to-c	0.021 ± 0.0064
MAM-CAuBP1	Au NP	c-to-t	0.031 ± 0.0042
AuBP1C-MAM	Au NP	t-to-c	0.014 ± 0.001
AuBP1C-MAM	Au NP	c-to-t	0.024 ± 0.0071
AuBP1C-MAM	5 nm Au NP	t-to-c	0.011± 0.0046
AuBP1C-MAM	5 nm Au NP	c-to-t	0.021 ± 0.0053
MAM-CAuBP1	Ag NP	t-to-c	0.029 ± 0.0053
MAM-CAuBP1	Ag NP	c-to-t	0.032 ± 0.0058
AuBP1C-MAM	Ag NP	t-to-c	0.03 ± 0.0012
AuBP1C-MAM	Ag NP	c-to-t	0.038 ± 0.0066

Table S2: Residue-surface contact data (percentage) on Au. The "c" or "t" in front of the MAM refers to the *cis* or *trans* conformation of the MAM. Anchor residues (with a contact percentage ≥ 60%) are highlighted. *Previous work.[7]

Residue	tMAM-CAuBP1	cMAM-CAuBP1	AuBP1C-tMAM	AuBP1-cMAM	AuBP1*
MAM	99.7	87.9	---	---	---
CYS	86.4	69.0	---	---	---
TRP	84.2	78.0	92.7	82.0	84
ALA	7.0	21.6	15.9	34.3	48
GLY	32.2	36.2	43.6	55.5	66
ALA	36.1	49.0	13.6	60.4	58
LYS	35.0	31.6	23.9	26.6	22
ARG	74.5	43.1	83.9	87.0	92
LEU	14.0	38.6	16.3	47.7	46
VAL	46.1	33.7	69.3	24.4	39
LEU	18.1	39.9	22.4	22.0	49
ARG	38.2	61.3	62.8	58.0	77
ARG	73.0	76.4	72.6	64.3	85
GLU	47.1	39.2	26.1	41.0	50
CYS	---	---	99.8	65.2	---
MAM	---	---	99.9	94.4	---

Table S3: Residue-surface contact data (percentage) on Ag. The "c" or "t" in front of the MAM refers to the *cis* or *trans* conformation of the MAM. Anchor residues (with a contact percentage ≥ 60%) are highlighted. *Previous work.[7]

Residue	tMAM-CAuBP1	cMAM-CAuBP1	AuBP1C-tMAM	AuBP1-cMAM	AuBP1*
MAM	89.3	22.4	---	---	---
CYS	87.0	17.1	---	---	---
TRP	18.7	32.4	20.5	2.4	44
ALA	27.4	19.7	3.2	7.5	17
GLY	33.9	44.5	3.3	3.6	45
ALA	44.8	32.0	23.2	5.4	38
LYS	6.6	4.5	7.6	14.8	53
ARG	24.9	41.1	17.3	25.2	47
LEU	2.9	12.8	4.4	2.7	29
VAL	5.3	25.4	19.0	7.9	66
LEU	9.7	5.7	28.0	23.5	46
ARG	12.5	20.6	40.8	33.9	76
ARG	25.0	48.3	35.9	43.0	75
GLU	5.1	7.3	6.9	5.2	4
CYS	---	---	76.5	69.1	---
MAM	---	---	83.3	55.5	---

Table S4: Residue-surface contact data (percentage) of the Cys and the five reference points of the MAM. The "c" or "t" in front of the MAM refers to the *cis* or *trans* conformation of the MAM. MAL refers to the center of mass of the maleimide ring, AZB to the center of mass of the phenyl ring, and N=N to the mid-point of the N=N bond. The label "1" is used to denote the rings that are closer to the Cys, and the label "2" for the rings that are found at the far end of the chain. Anchor residues (with a contact percentage ≥ 60%) are highlighted.

Au				
Site	tMAM-CAuBP1	cMAM-CAuBP1	AuBP1C-tMAM	AuBP1-cMAM
CYS	86.4	69.0	99.8	65.2
MAL1	79.8	62.2	96.9	86.7
AZB1	99.8	47.3	100.0	8.0
N=N	99.7	87.9	99.9	94.4
AZB2	99.8	44.8	100.0	89.6
MAL2	98.4	94.2	98.0	94.9
Ag				
Site	tMAM-CAuBP1	cMAM-CAuBP1	AuBP1C-tMAM	AuBP1-cMAM
CYS	87.0	17.1	76.5	69.1
MAL1	65.0	31.0	78.2	87.7
AZB1	89.3	18.4	83.1	40.0
N=N	89.3	22.4	83.3	55.5
AZB2	89.3	9.5	83.4	16.2
MAL2	89.3	89.4	87.0	80.0

Table S5: Percentage population of the top ten most populated clusters of single chain of AuBP1 adsorbed at the aqueous Au and Ag interfaces respectively, reproduced from Tang et al.[20] and Palafox-Hernandez et al.[19]

	AuBP1	
Cluster	AU	AG
1	21.3	15.9
2	14.2	12.0
3	13.8	11.2
4	12.1	8.8
5	4.0	7.5
6	3.5	5.1
7	3.3	4.9
8	2.8	3.2
9	2.6	2.6
10	2.3	2.4

Table S6: Percentage population of the top ten most populated clusters of the hybrid molecule adsorbed at the aqueous Au and Ag interfaces. The "c" or "t" in front of the MAM refers to the *cis* or *trans* conformation of the MAM. Data for the Au surface are reproduced from Tang et al.[13]

	AU			
Cluster	NC-tMAM	CC-tMAM	NC-cMAM	CC-cMAM
1	28.7	29.4	20.3	24.5
2	15.9	17.9	11.4	13.6
3	11.9	10.1	8.3	10.3
4	7.5	7.1	8.1	9.3
5	4.9	5.2	6.6	7.7
6	3.6	5.2	6.5	4.4
7	3.1	3.5	6.3	3.4
8	3.0	2.8	4.4	2.9
9	2.6	2.2	3.1	2.7
10	2.1	1.9	2.9	2.3
	AG			
Cluster	NC-tMAM	CC-tMAM	NC-cMAM	CC-cMAM
1	20.5	16.4	26.6	13.4
2	9.8	11.5	10.3	9.0
3	8.8	9.1	6.6	5.1
4	8.7	5.4	6.1	4.4
5	5.7	5.0	5.8	4.1
6	5.1	4.3	5.4	3.7
7	4.4	3.5	5.3	3.7
8	4.3	3.5	3.5	3.6
9	2.6	3.4	3.3	3.1
10	2.1	2.4	2.4	3.0

Table S7: Comparison of cluster centroids, comparing the AuBP1 peptide backbone structure on Au and Ag surfaces. A matched peptide conformation has a RMSD lower than 0.2 nm. The columns under the AU and AG headings give the cluster rank in each case.

AuBP1 parent		
AU	AG	RMSD (nm)
1	2	0.179
1	14	0.186
1	23	0.179
2	50	0.187
2	67	0.195
4	6	0.170
4	31	0.155
5	5	0.170
5	9	0.137
5	38	0.172
5	44	0.199
7	17	0.186
7	26	0.193
7	32	0.182
9	76	0.197
10	16	0.189

Table S8: Comparison of cluster centroids, comparing the AuBP1 backbone structure as part of the hybrid molecules, adsorbed on Au and Ag surfaces. A matched peptide conformation has a RMSD lower than 0.2 nm. The columns under the Au and Ag headings give the cluster rank in each case. The "c" or "t" in front of the MAM refers to the *cis* or *trans* conformation of the MAM. Pairs with a backbone RMSD less than or equal to the clustering cutoff ("matched" structures) are highlighted in yellow.

NC-tMAM			NC-cMAM		
Au	Ag	RMSD, nm	Au	Ag	RMSD, nm
1	61	0.186	2	79	0.184
1	65	0.174	3	10	0.174
2	43	0.199	3	27	0.197
2	65	0.199	3	60	0.196
6	61	0.195	4	4	0.184
7	69	0.179	4	19	0.177
8	44	0.181	6	9	0.190
9	70	0.174	6	17	0.175
10	75	0.188	7	23	0.196
10	103	0.197	8	10	0.199
-	-	-	8	60	0.196
CC-tMAM			CC-cMAM		
Au	Ag	RMSD, nm	Au	Ag	RMSD, nm
1	24	0.146	1	65	0.194
2	14	0.183	1	92	0.199
3	4	0.176	2	76	0.166
3	108	0.192	2	152	0.195
4	34	0.156	3	10	0.178
4	63	0.136	3	114	0.183
4	135	0.186	6	4	0.175
5	111	0.181	6	18	0.197
5	112	0.188	6	122	0.175
6	21	0.198	7	3	0.196
6	39	0.186	7	13	0.198
7	13	0.191	8	11	0.160
7	94	0.199	8	89	0.181
8	5	0.158	-	-	-
8	139	0.191	-	-	-
9	14	0.189	-	-	-

Table S9: Comparison of cluster centroids, comparing the AuBP1 backbone structure as part of the hybrid molecules with the parent AuBP1 peptide, adsorbed on the Au surface. A matched peptide conformation has a RMSD lower than 0.2 nm. The columns under the AU headings give the cluster rank in each case. The "c" or "t" in front of the MAM refers to the *cis* or *trans* conformation of the MAM. Pairs with a backbone RMSD less than or equal to the clustering cutoff ("matched" structures) are highlighted in yellow.

	AU			AU	
PARENT	NC-tMAM	RMSD nm	PARENT	NC-cMAM	RMSD nm
1	46	0.176	1	4	0.124
5	49	0.182	1	15	0.194
-	-	-	1	34	0.163
-	-	-	2	39	0.158
-	-	-	4	10	0.172
-	-	-	5	6	0.165
-	-	-	5	32	0.186
-	-	-	6	43	0.131
-	-	-	7	20	0.184
-	-	-	10	18	0.187
-	-	-	10	54	0.193
	AU			AU	
PARENT	CC-tMAM	RMSD nm	PARENT	CC-cMAM	RMSD nm
1	13	0.190	1	6	0.199
2	2	0.180	1	14	0.190
3	27	0.180	1	32	0.177
3	68	0.168	2	1	0.174
4	1	0.175	2	9	0.162
5	16	0.192	2	37	0.192
5	31	0.168	4	7	0.187
7	32	0.191	5	2	0.193
8	4	0.188	5	14	0.190
-	-	-	5	44	0.166
-	-	-	5	59	0.189
-	-	-	5	77	0.152
-	-	-	10	10	0.196
-	-	-	10	37	0.198

Table S10: Comparison of cluster centroids, comparing the AuBP1 backbone structure as part of the hybrid molecules with the parent AuBP1 peptide, adsorbed on the Ag surface. A matched peptide conformation has a RMSD lower than 0.2 nm. The columns under the AG headings give the cluster rank in each case. The "c" or "t" in front of the MAM refers to the *cis* or *trans* conformation of the MAM. Pairs with a backbone RMSD less than or equal to the clustering cutoff ("matched" structures) are highlighted in yellow.

PARENT	AG NC-tMAM	RMSD nm	PARENT	AG NC-cMAM	RMSD nm
1	8	0.142	1	43	0.197
1	13	0.195	2	4	0.191
1	20	0.198	2	30	0.177
5	42	0.182	2	49	0.180
5	47	0.188	2	95	0.196
6	3	0.175	5	10	0.190
6	66	0.194	5	23	0.153
6	95	0.194	7	4	0.194
7	70	0.198	7	19	0.195
8	26	0.185	7	22	0.197
8	69	0.175	7	49	0.185
9	42	0.166	8	26	0.189
10	18	0.197	9	9	0.188
PARENT	AG CC-tMAM	RMSD nm	PARENT	AG CC-cMAM	RMSD nm
1	14	0.195	1	152	0.1878
1	55	0.196	2	31	0.1857
2	119	0.183	2	54	0.1644
2	132	0.160	2	76	0.1954
3	42	0.191	2	92	0.1835
3	101	0.169	3	21	0.1888
4	5	0.177	5	16	0.1791
4	53	0.188	5	47	0.1692
5	14	0.179	5	56	0.1978
5	24	0.190	6	56	0.1561
5	34	0.181	7	4	0.1532
5	63	0.169	7	65	0.1415
5	85	0.185	7	122	0.1464
6	138	0.178	9	16	0.1557
7	1	0.190	10	69	0.1969
7	13	0.147	-	-	-
7	30	0.180	-	-	-
7	94	0.185	-	-	-
8	15	0.175	-	-	-
9	63	0.196	-	-	-
9	71	0.196	-	-	-
9	85	0.157	-	-	-

Table S11: Comparison of cluster centroids, comparing the AuBP1 backbone structure as part of the hybrid molecules, adsorbed on the Au surface. A matched peptide conformation has a RMSD lower than 0.2 nm. The columns under the tMAM and cMAM headings give the cluster rank in each case. The "c" or "t" in front of the MAM refers to the *cis* or *trans* conformation of the MAM. Pairs with a backbone RMSD less than or equal to the clustering cutoff ("matched" structures) are highlighted in yellow.

NC / AU			CC / AU		
tMAM	cMAM	RMSD nm	tMAM	cMAM	RMSD nm
6	7	0.163	1	7	0.159
6	20	0.170	1	27	0.155
8	64	0.187	2	6	0.195
9	15	0.179	2	19	0.176
10	59	0.187	2	37	0.139
-	-	-	3	63	0.161
-	-	-	4	7	0.193
-	-	-	5	65	0.199
-	-	-	6	30	0.168
-	-	-	7	6	0.197
-	-	-	7	32	0.193
-	-	-	8	20	0.180
-	-	-	9	13	0.190
-	-	-	9	19	0.169
NC SILVER			CC SILVER		
tMAM	cMAM	RMSD nm	tMAM	cMAM	RMSD nm
2	16	0.169	1	4	0.182
4	19	0.190	1	65	0.168
6	79	0.194	1	122	0.120
8	12	0.194	3	45	0.170
8	41	0.191	3	70	0.199
8	71	0.194	4	2	0.145
9	37	0.186	6	31	0.196
10	16	0.195	8	69	0.182
10	38	0.185	9	29	0.178
10	54	0.172	9	107	0.199
-	-	-	9	146	0.186

Table S12: Comparison of cluster centroids, comparing the AuBP1 backbone structure as part of the hybrid molecules, adsorbed on the Au and Ag surfaces. A matched peptide conformation has a RMSD lower than 0.2 nm. The columns under the NC and CC headings give the cluster rank in each case. The "c" or "t" in front of the MAM refers to the *cis* or *trans* conformation of the MAM. Pairs with a backbone RMSD less than or equal to the clustering cutoff ("matched" structures) are highlighted in yellow.

tMAM / AU			tMAM / AG		
NC	CC	RMSD nm	NC	CC	RMSD nm
1	3	0.108	2	20	0.182
2	7	0.132	2	93	0.191
2	29	0.193	3	4	0.196
6	3	0.159	3	96	0.199
6	14	0.163	3	138	0.178
6	32	0.160	4	13	0.169
8	34	0.153	4	29	0.142
8	60	0.198	5	23	0.164
8	65	0.183	5	37	0.182
-	-	-	5	144	0.193
-	-	-	7	40	0.181
-	-	-	8	86	0.189
-	-	-	10	6	0.191
cMAM / AU			cMAM / AG		
NC	CC	RMSD nm	NC	CC	RMSD nm
1	17	0.191	1	58	0.166
2	6	0.188	1	140	0.174
3	8	0.197	2	149	0.181
3	12	0.195	3	44	0.190
3	16	0.199	3	122	0.199
4	41	0.176	4	4	0.179
4	48	0.198	6	117	0.188
6	2	0.190	7	75	0.184
6	14	0.196	7	100	0.191
6	44	0.167	7	113	0.187
6	59	0.183	7	150	0.187
6	77	0.139	8	81	0.195
7	7	0.183	8	125	0.191
7	13	0.180	9	16	0.199
8	25	0.190	10	5	0.190
-	-	-	10	144	0.194

Table S13: Conformational entropy contribution calculated using the discrete entropy (Equation 1, main text) evaluated for both the entire hybrid molecule (Whole), and for the AuBP1 subset of the hybrid molecule, adsorbed at the aqueous Au and Ag interfaces. Values taken from previous work[7] for the parent peptide adsorbed at these interfaces are provided for convenience.

Compound	**Au(111)**		**Ag(111)**	
AuBP1*	2.56		2.73	
Comp\Reference	Whole	AuBP1	Whole	AuBP1
cMAM-CAuBP1	3.50	2.89	3.41	2.97
AuBP1C-cMAM	3.20	2.73	3.69	3.73
tMAM-CAuBP1	2.71	2.58	3.23	3.14
AuBP1C-tMAM	2.86	2.52	3.37	3.43

References

1. Barducci, A.; Bussi, G.; Parrinello, M., Well-tempered metadynamics: A smoothly converging and tunable free-energy method. *Phys Rev Lett* **2008,** *100* (2).

2. Bonomi, M.; Branduardi, D.; Bussi, G.; Camilloni, C.; Provasi, D.; Raiteri, P.; Donadio, D.; Marinelli, F.; Pietrucci, F.; Broglia, R. A.; Parrinello, M., PLUMED: A portable plugin for free-energy calculations with molecular dynamics. *Comput Phys Commun* **2009,** *180* (10), 1961-1972.

3. Nose, S., A Molecular-Dynamics Method for Simulations in the Canonical Ensemble. *Mol Phys* **1984,** *52* (2), 255-268.

4. Hoover, W. G., Canonical dynamics: Equilibrium phase-space distributions. *Physical Review A* **1985,** *31*, 1695 - 1697.

5. Hess, B.; Kutzner, C.; van der Spoel, D.; Lindahl, E., GROMACS 4: Algorithms for highly efficient, load-balanced, and scalable molecular simulation. *J Chem Theory Comput* **2008,** *4* (3), 435-447.

6. Wright, L. B.; Rodger, P. M.; Corni, S.; Walsh, T. R., GoIP-CHARMM: First-Principles Based Force Fields for the Interaction of Proteins with Au(111) and Au(100). *J Chem Theory Comput* **2013,** *9* (3), 1616-1630.

7. Wright, L. B.; Rodger, P. M.; Walsh, T. R.; Corni, S., First-Principles-Based Force Field for the Interaction of Proteins with Au(100)(5 x 1): An Extension of GoIP-CHARMM. *J Phys Chem C* **2013,** *117* (46), 24292-24306.

8. Hughes, Z. E.; Wright, L. B.; Walsh, T. R., Biomolecular Adsorption at Aqueous Silver Interfaces: First-Principles Calculations, Polarizable Force-Field Simulations, and Comparisons with Gold. *Langmuir* **2013,** *29* (43), 13217-13229.

9. MacKerell, A. D.; Bashford, D.; Bellott, M.; Dunbrack, R. L.; Evanseck, J. D.; Field, M. J.; Fischer, S.; Gao, J.; Guo, H.; Ha, S.; Joseph-McCarthy, D.; Kuchnir, L.; Kuczera, K.; Lau, F. T. K.; Mattos, C.; Michnick, S.; Ngo, T.; Nguyen, D. T.; Prodhom, B.; Reiher, W. E.; Roux, B.; Schlenkrich, M.; Smith, J. C.; Stote, R.; Straub, J.; Watanabe, M.; Wiorkiewicz-Kuczera, J.; Yin, D.; Karplus, M., All-atom empirical potential for molecular modeling and dynamics studies of proteins. *J Phys Chem B* **1998,** *102* (18), 3586-3616.

10. Piana, S.; Lindorff-Larsen, K.; Shaw, D. E., How Robust Are Protein Folding Simulations with Respect to Force Field Parameterization? *Biophys J* **2011,** *100* (9), L47-L49.

11. Jorgensen, W. L.; Chandrasekhar, J.; Madura, J. D.; Impey, R. W.; Klein, M. L., Comparison of Simple Potential Functions for Simulating Liquid Water. *J Chem Phys* **1983,** *79* (2), 926-935.

12. Neria, E.; Fischer, S.; Karplus, M., Simulation of activation free energies in molecular systems. *J Chem Phys* **1996,** *105* (5), 1902-1921.

13. Tang, Z. H.; Lim, C.-K.; Palafox-Hernandez, J. P.; Drew, K. L. M.; Li, Y.; Swihart, M. T.; Prasad, P. N.; Walsh, T. R.; Knecht, M. R., Triggering Nanoparticle Surface Ligand Rearrangement via External Stimuli: Light-based Actuation of Biointerfaces. *Nanoscale* **2015,** *DOI: 10.1039/C5NR02311D*.

14. Darden, T.; York, D.; Pedersen, L., Particle Mesh Ewald - an N.Log(N) Method for Ewald Sums in Large Systems. *J Chem Phys* **1993,** *98* (12), 10089-10092.

15. Wright, L. B.; Freeman, C. L.; Walsh, T. R., Benzene adsorption at the aqueous (011) alpha-quartz interface: is surface flexibility important? *Mol Simulat* **2013,** *39* (13), 1093-1102.

16. Terakawa, T.; Kameda, T.; Takada, S., On Easy Implementation of a Variant of the Replica Exchange with Solute Tempering in GROMACS. *J Comput Chem* **2011,** *32* (7), 1228-1234.

17. Wright, L. B.; Walsh, T. R., Efficient conformational sampling of peptides adsorbed onto inorganic surfaces: insights from a quartz binding peptide. *Phys Chem Chem Phys* **2013,** *15* (13), 4715-4726.

18. Daura, X.; Gademann, K.; Jaun, B.; Seebach, D.; van Gunsteren, W. F.; Mark, A. E., Peptide folding: When simulation meets experiment. *Angew Chem Int Edit* **1999,** *38* (1-2), 236-240.

19. Palafox-Hernandez, J. P.; Tang, Z. H.; Hughes, Z. E.; Li, Y.; Swihart, M. T.; Prasad, P. N.; Walsh, T. R.; Knecht, M. R., Comparative Study of Materials-Binding Peptide Interactions with Gold and Silver Surfaces and Nanostructures: A Thermodynamic Basis for Biological Selectivity of Inorganic Materials. *Chem Mater* **2014,** *26* (17), 4960-4969.

20. Tang, Z. H.; Palafox-Hernandez, J. P.; Law, W. C.; Hughes, Z. E.; Swihart, M. T.; Prasad, P. N.; Knecht, M. R.; Walsh, T. R., Biomolecular Recognition Principles for Bionanocombinatorics: An Integrated Approach To Elucidate Enthalpic and Entropic Factors. *Acs Nano* **2013,** *7* (11), 9632-9646.